Lawrence Berkeley National Laboratory

Title

Effects of surface orientation, fluid chemistry and mechanical polishing on the variability of dolomite dissolution rates

Permalink

https://escholarship.org/uc/item/17z889hm

Authors

Saldi, Giuseppe D
Voltolini, Marco
Knauss, Kevin G

Publication Date

2017-06-01

DOI

10.1016/j.gca.2017.02.007

Copyright Information

Peer reviewed

Effects of surface orientation, fluid chemistry and mechanical polishing on the variability of dolomite dissolution rates

Giuseppe D. Saldi *, Marco Voltolini, Kevin G. Knauss

Earth and Environmental Sciences, Lawrence Berkeley National Laboratory, 1 Cyclotron Road, Berkeley, CA 94720, USA

Abstract

Recent studies of carbonate surface reactivity have underscored the fundamental variability of dissolution rates and the heterogeneous distribution of the reaction over the mineral surface due to the inhomogeneous distribution of surface energy. Dolomite dissolution rates relative to different cleavage planes (*r*-planes) and surfaces cut approximately perpendicular to the *c*-axis (*c*-planes) were studied at 50 °C as a function of pH (3.4 ≤ pH ≤ 9.0) and solution composition by vertical scanning interferometry (VSI) and atomic force microscopy (AFM), with the aim of providing an estimate of the intrinsic rate variation of dolomite single crystals and describing the surface reaction distribution and the rate controlling mechanisms. Surface normal retreat rates measured under acidic conditions increased linearly with time and were not visibly affected by the parallel increase of surface roughness. Mean total dissolution rates of *r*-planes decreased by over 200 times from pH 3.4 to pH 9.0 and CO_3^{2-}-rich solutions, whereas corresponding rate variations spanned over 3 orders of magnitude when also *c*-plane rate distributions were included in the analysis. At acid to near neutral pH, *c*-planes dissolved ∼ three times faster than the adjoining *r*-planes but slower at basic pH and high total carbon concentration, displaying a distinctive morphologic evolution in these two regimes. The comparison of polished and unpolished crystals showed that polished cleavage planes dissolved about three times faster than the unpolished counterpart at near neutral to basic conditions, whereas no significant difference in reactivity was observed at pH < 5.

Although experimental data and observations indicate a tendency of dolomite faces to reach a low-energy topography over the course of the reaction, the evolution of the entire crystal morphology depends also on the reactivity of edge and corner regions, whose contribution to measured rates is not generally taken into account by laboratory experiments. The study of time-dependent mineral morphology and reactivity requires an integrated approach of kinetic modeling and experimentation, where measured rate variance and observed reaction mechanisms represent fundamental parameters for the improvement of geochemical models in predicting long-term reaction rates in a wide range of environmental conditions.
© 2017 Elsevier Ltd. All rights reserved.

Keywords: Dolomite dissolution; Vertical scanning interferometry; Atomic force microscopy; Rate spectra; Reactive surface area; Surface topography; Rate variability; Mechanical polishing

1. INTRODUCTION

The extent to which mineral dissolution rates involved in various industrial processes and long-term weathering reactions can be accurately predicted depends on the knowledge of the fundamental mechanisms that take place at the

* Corresponding author at: GET, CNRS/UMR 5563-Université Paul Sabatier, 14 ave. E. Belin, 31400 Toulouse, France.
E-mail addresses: gdsaldi@lbl.gov, giuseppe.saldi@get.omp.eu (G.D. Saldi).

mineral-fluid interface and on the understanding of the effects that the complex interplay of different physicochemical parameters, such as temperature, pH, pCO_2, chemical composition of the fluid, presence of organic ligands, and the crystallographic and microstructural features of reactive surfaces, exerts on these reactions (cf. White and Brantley, 2003; Maher et al., 2009; Voltolini et al., 2012; Lüttge et al., 2013). Although large discrepancies generally exist between field-derived rates and laboratory measurements, the comparison of various experimental data also reveal the existence of significant variations in measured laboratory rates (cf. Arvidson et al., 2003; Beig and Lüttge, 2006; Lüttge et al., 2013). The origin of such differences mostly resides in the intrinsic variability of surface reactivity, which reflects the heterogeneous distribution of surface defects and active sites, and possibly the variation of grain size and grain-boundary density of the investigated solids (cf. Arvidson et al., 2003; Fischer et al., 2012, 2014). Clear evidence of the intrinsic variability of measured dissolution rates is provided by recent high-resolution studies conducted on single crystal surfaces by atomic force microscopy (AFM), optical profilometry [confocal profilometry (CP), phase-shift interferometry (PSI) and vertical scanning interferometry (VSI)] and other complementary techniques (e.g., Fischer et al., 2012; Godinho et al., 2012; Daval et al., 2013; King et al., 2014; Pollet-Villard et al., 2016), which illustrate the dependence of measured surface retreat rates on the crystallographic orientation, the physico-chemical microstructure of the investigated planes as well as the exposure time to the reactive fluid.

Knowledge of such inherent variability is particularly relevant within the carbonate system given the fundamental implication of major carbonate minerals (calcite and dolomite) in a wide variety of geological processes. The dissolution of calcite and dolomite plays an essential role in the regulation of the long-term C cycle (Berner et al., 1983; Mackenzie and Andersson, 2013) and significantly affects pH and alkalinity of natural waters; it controls the levels of trace metals released into groundwater (see Apps et al., 2010; Wunsch et al., 2013) and allows the development of carbonate reservoirs influencing their productivity (Worthington and Ford, 2009).

Many AFM and VSI studies were carried out over the last two decades to describe the elementary processes that control the dissolution of carbonate minerals, specifically investigating the formation of etch pits and the kinematics of monolayer steps under a wide variety of experimental conditions (e.g., Liang and Baer, 1997; Jordan and Rammensee, 1998; Shiraki et al., 2000; Lea et al., 2001; Higgins et al., 2002; Lüttge et al., 2003; Teng, 2004; Bisschop et al., 2006; Urosevic et al., 2012; Smith et al., 2013; Emmanuel, 2014). However, most of these works reported observations made on limited areas of the $\{10\bar{1}4\}$ cleavage surfaces and for relatively short experimental durations (typically ranging from a few minutes to several hours), so that the long-term evolution of representative portions of the mineral surface and the corresponding rates and distribution of the dissolution reaction were not adequately examined.

A limited number of publications looked at the influence of the crystallographic orientation and the effects of polishing and applied stress on the dissolution mechanisms of calcite. It was shown that the dissolution rates of calcite surfaces increase with the angle of miscut with respect to the $\{10\bar{1}4\}$ cleavage planes (Compton et al., 1986; Bisschop et al., 2006) but such difference decreases with increasing aqueous solution saturation (Smith et al., 2013). Schott et al. (1989) and MacInnis and Brantley (1992) reported an increase of dissolution rates by a factor of 2–3 for the cleavage planes of strained calcite samples whereas the rate dependence on dislocation density was generally found to be weak.

There have been few studies conducted on dolomite surface reactivity with atomic to nano-scale resolution compared to calcite (Lüttge et al., 2003; Higgins and Hu, 2005; Hu et al., 2005; Fenter et al., 2007; Kaczmarek and Sibley, 2007; Ruiz-Agudo et al., 2011; Urosevic et al., 2012; Xu et al., 2013; Putnis et al., 2014) and, although a notable progress in the understanding of the mechanisms and rates that control dolomite dissolution has been achieved, the complex nature of this mineral still requires detailed investigations to get to a more comprehensive picture of the processes that control its reactivity and formation in natural environments (cf. Kaczmarek and Sibley, 2014).

In this study we examine the effects of crystallographic orientation, pH and presence of defects generated by polishing on the mean rates of dolomite dissolution and the corresponding distribution of dissolution fluxes over the mineral surface with the two main objectives of: (i) providing experimental data that contribute to a more representative characterization of dolomite dissolution mechanisms and rates as a function of time and aqueous solution composition; (ii) improving our general understanding of mineral surface reactivity to help the advancement of modern computational tools in predicting long-term weathering reactions at the field-scale. The evolution of surface micro-topography and the surface normal retreats of mm-sized dolomite crystals were analyzed on both the $\{10\bar{1}4\}$ cleavage planes and miscut surfaces approximately parallel to the $\{0001\}$ crystallographic form. Because of the different morphologic characteristics and the different surface energies associated with these two planes, the analysis and comparison of their reactivity allow the description of the amplitude of dolomite rate variations and provide data that serve to model the evolution of the surface area of crystal grains as a function of time.

To express the observed variance of dissolution rates, recent AFM and VSI studies on calcite and dolomite (Fischer et al., 2012; Emmanuel, 2014; Emmanuel and Levenson, 2014) proposed the use of rate spectra providing information on range and distribution of surface dissolution fluxes and the frequency of corresponding energetic sites, as opposed to the use of single mean rate values obtained by traditional surface area normalization operations, which do not allow the description of the effects of these parameters on the intrinsic reaction rate variation. The use of this analytical tool is therefore of great relevance

for the accurate description and modeling of mineral surface reactivity and will be employed to illustrate our results.

2. EXPERIMENTAL

2.1. Dolomite crystals preparation

Several dolomite single crystals of high optical quality, with an average size of 3 to 5 mm, were prepared by cleaving a dolomite sample from Eugui (Navarra, Spain) parallel to the natural $\{10\bar{1}4\}$ cleavage planes. Electron microprobe analyses of this sample provided the following chemical composition by weight: $MgO = 20.96 \pm 0.32\%$, $CaO = 30.53 \pm 0.23\%$, $FeO = 0.71 \pm 0.18\%$ and $MnO = 0.08 \pm 0.03\%$. These results are in very good agreement with the data obtained by bulk chemical analyses (performed by total fusion, ICP-OES and IR analyses at Activation Laboratories, Ancaster, Canada): $MgO = 21.24 \pm 0.1\%$, $CaO = 29.95 \pm 0.1\%$, $FeO = 1.00 \pm 0.2\%$, $MnO = 0.09 \pm 0.001\%$ and $CO_2 = 46.9 \pm 0.3\%$. The average chemical composition resulting from these analyses is consistent with the following recalculated dolomite formula: $Ca_{1.0}Mg_{0.99}Fe_{0.01}(CO_3)_2$.

A number of the obtained rhombohedral crystals were polished on three adjacent cleavage faces while a miscut surface, approximately perpendicular to the c-axis ([001] crystallographic orientation) was also cut and polished to study the evolution of the surface topography and the vertical retreat in comparison with the $\{10\bar{1}4\}$ cleavage surfaces. The polishing procedure was carried out on already cleaved crystal samples. The samples were mounted onto a dop of a faceting machine (XS3) equipped with a digital goniometer with a theoretical precision of $\sim 0.02°$. Pitch and roll angles of the polishing arm were adapted to accommodate the flat, cleaved surface, onto the polishing lap. Once the crystal and lap surfaces were parallel, the two angles were locked in place and kept constant during the polishing procedure. This alignment procedure was carried out for each $\{10\bar{1}4\}$ surface. The polishing procedure was performed in two stages: first, a pre-polish using 3000 grit diamond powder with WD40 fluid extender on a tin alloy lap was done to polish out the visible steps. Finally a polishing stage using 100.000 grit diamond on a tin alloy lap (~ 400 rpm speed) was done to assure a flatter and better polished surface. The pre-polish and polish procedures were carried out on cleaned tin alloy laps, meaning that the polishing agent was distributed, then forced into the lap surface using a flat piece of synthetic corundum, and then cleaned with a paper towel. This procedure ideally results in embedded particles in the metal matrix, and no loose particles, assuring a smaller effective scratch size with no rolling action of the grit particles at the crystal-lap interface. The choice of using a metal polishing lap was also made to minimize the heating of the sample: polishing generates heat, and a highly thermally conductive material, such as the used tin alloy, acts as a heat sink and efficiently dissipates any generated heat. The $\{0001\}$ surfaces were cut and polished with the same procedure, adding to the jaw angle 43.9 degrees from the last rhombohedral face polishing setting. The RMS roughness (R_q) of pristine polished surfaces, as measured by vertical scanning interferometry (VSI) for a field of view (FOV) of 692 μm × 518 μm, was generally lower than 200 nm (see Section 4.2).

A few crystals were only cut parallel to the $\{10\bar{1}4\}$ form and used without any chemical or mechanical treatment to assess the effects of roughness and initial cleavage-induced topography vs. polishing on the measured rates of dissolution and the associated topography development. For sake of simplicity, we will refer to the main $\{10\bar{1}4\}$ cleavage surfaces as r-planes and to the surfaces parallel to the $\{0001\}$ orientation as c-planes, in agreement with the notation used by Smith et al. (2013).

2.2. Experimental setup and surface measurements

Experiments were carried out in a thermostatic bath at $50 \pm 1\,°C$ using 120 ml PFA containers by Savillex, which were assembled to perform as reactors in flow-through mode. At the beginning of each experiment, one or two dolomite single-crystals were placed inside one of the reactors, where the experimental solution was previously circulated for some time while the temperature of the system attained 50 °C. The reactor was opened just to introduce the dolomite crystals, then closed and immediately put back in the thermostatic bath. The experiments were conducted with a fluid flow rate of 0.5 ml/min using a Gilson Minipuls peristaltic pump and the solution in the reactors was continuously mixed using a suspended magnetic stirrer rotating at a constant speed of 350 rpm. The duration of the experiments varied between 1 and 30 days (Table 1). At the end of each run, the dolomite crystals were recovered and rinsed for several seconds in deionized water and in ethanol and then dried in an oven at 50 °C before surface analyses.

Aqueous fluids of different pH's and aqueous carbonate concentrations were prepared by mixing variable amounts of HCl, $NaHCO_3$, NaOH, CH_3COONa and NaCl while keeping the total electrolyte (Na) concentration at a constant value of 0.01 M. The list of the experiments and the aqueous solution compositions used in this study are given in Table 1.

To measure the vertical surface retreat due to the dissolution reaction, selected portions of the crystal surface were prevented from dissolving by physically masking these areas using both Viton discs and silicone glue spots (Fig. 1), according to the methods described by Arvidson et al. (2004) and Daval et al. (2013). These protections were removed from the surface at the end of the experiments, or after each reaction step, so that the masked, unreacted areas of the analyzed samples provided the reference surface against which changes in vertical surface height and topography were measured and corresponding dissolution rates were calculated (refer to Arvidson et al. (2004) for a description of the rate calculation method). The changes in topography and surface retreat were measured by vertical scanning interferometry (VSI) using a Zygo New View 7300 interferometer equipped with 10× and 50× Mirau objectives, with a maximum horizontal resolution of 100 nm and a vertical resolution of ~ 0.1 nm. Topographic data of different regions of analyzed crystal surfaces were obtained using different FOV's and resolutions. In particu-

Table 1
Summary of the single crystal flow-through experiments and corresponding aqueous solution compositions used in this study. The pH of the aqueous solutions was adjusted to the desired value by addition of small amounts of HCl or NaOH not indicated in the table. Note that: runs # DT2A–C refer to three distinct reaction steps conducted on the same crystal under identical conditions; DT-1 and DT-6 were conducted in different time steps to study the r-plane and c-plane retreat change as a function of time.

Run #	Investigated planes	Polishing	Number of Faces studied	Starting pH (20 °C)	NaCl mM	NaHCO$_3$ mM	NaAcet mM	Duration (days)
DT-1	(104)	No	1	4.45	10	0	0	3.9
DT-2A	(104), (001)	Yes	4	4.44	10	0	0	4.2
DT-2B	(104), (001)	Yes	4	4.44	10	0	0	5.0
DT-2C	(104), (001)	Yes	4	4.44	10	0	0	5.0
DT-3	(104), (001)	Yes	4	9.05	6	4	0	4.1
DT-4	(104), (001)	Yes	4	8.10	9	1	0	8.0
DT-5	(104), (001)	Yes/no	4/1[a]	9.05	6	4	0	30
DT-6	(001)	Yes	1	4.43	10	0	0	8.3
DT-7	(104)	No	1	4.43	10	0	0	3.8
DT-8	(104)	Yes/no	4/1[a]	5.47	7.5	0	2.5	5.0
DT-9	(104)	Yes/no	2/3[a]	4.45	10	0	0	4.0
DT-10	(104)	Yes	3	3.27	10	0	0	3.2
DT-11	(104), (001)	Yes	4	3.27	10	0	0	0.9

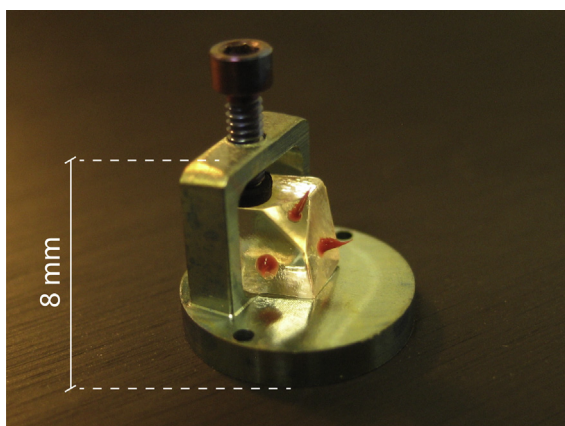[a] the second figure corresponds to an unpolished crystal: only $\{10\bar{1}4\}$ planes were analyzed.

Fig. 1. Dolomite single crystal and homemade Ti-jig serving as sample-holder for the dissolution experiments. The crystal shows four polished faces covered with red silicone glue spots and a Viton disc (top face) to protect a portion of each face against dissolution and provide a reference level to calculate the corresponding surface normal retreat after reaction. The crystal is held in place by pressing a Ti-screw down against the Viton disc on the upper face of the crystal. (For interpretation of the references to color in this caption, the reader is referred to the web version of this article.)

lar, 3D-maps of the entire surface of the investigated crystal faces were acquired by operating the VSI in stitching mode (with a 20% overlap between successive frames) to get representative data of the spatial distribution of the dissolution reaction and to calculate the corresponding total rates of dissolution of different crystal faces. The total rate of dissolution is the sum of two different contributions (Arvidson et al., 2003): (i) the "global" retreat rate of the entire surface, as measured by the height difference across the edge of the masked region, and (ii) the "local" rate due to the local development of etch pits, which provide a supplementary volume of material removed by dissolution.

Additional surface topography characterization was accomplished by atomic force microscopy (AFM) to capture finer scale topographic details of the reacted surfaces, but without providing any supplementary information on measured surface normal retreats and rate distributions. A Digital Instruments Multimode AFM working in tapping mode with a Nanoscope IV control system was used for this purpose.

On previously polished dolomite crystals, average total surface retreat rates were calculated by measuring height differences between the unreacted reference surface and the dissolved surface along surface profiles typically taken along 4 different directions while averaging data over widths comprising between 100 and 150 data-lines. However, this method could not be applied successfully to unpolished dolomite faces because of their very rough topography. In this case surface vertical retreats were measured according to a void volume calculation, i.e., by subtracting the topography of the starting surface from that of the dissolved surface, after superimposition of the corresponding 3D-maps with respect to the same reference point retrieved on the protected portion of the analyzed surface. Total surface retreat rates were obtained by dividing the volume of material dissolved underneath the original surface topography by the reaction time and the selected surface area of analysis, the dimensions and shape of which were chosen to approximate those of the examined face of the crystal. This calculation was carried out using a computer routine developed with the software SPIP v6.3.3 by Image Metrology. The same procedure was also applied, whenever it was possible, to calculate total surface normal retreats of polished samples. The results obtained according to the two described methods (surface profiling and void volume calculation) were generally in good agreement, showing differences on the order of 4–10%. However, in some instances (particularly in the case of small global retreats and important topographic development) the void

volume calculation provided a more accurate estimate of the total retreat of the surface and the value obtained from this method was preferred to that obtained by vertical profile averaging.

2.3. Fluid sample analyses and thermodynamic calculations

Several aqueous samples were collected during the experiments, acidified with concentrated nitric acid and analyzed for Ca and Mg by ICP-OES (Varian 720 ES) to monitor the progress of the dissolution reaction in solution. All speciation and solubility calculations were carried out using the geochemical code PHREEQC v. 3.1 (Parkhurst and Appelo, 2013) using its LLNL thermodynamic database. Activity coefficients for dissolved species were calculated using the Debye-Hückel equation.

The degree of saturation of the aqueous solutions with respect to the minerals of interest are expressed in terms of saturation index, defined as the decimal logarithm of the ratio between the ion activity product of the reaction of mineral hydrolysis and the corresponding value of the solubility product [$SI = \log(IAP/K_{sp})$].

3. RESULTS

3.1. Surface normal retreat rates as a function of solution composition, surface orientation and time

A series of experiments were conducted to study the effect of pH and solution composition on the measured vertical retreats of dolomite cleavage surfaces (r-planes) and the surface cut parallel to the $\{0001\}$ plane orientation (c-plane). The measured retreats relative to three different experiments conducted at an increasing pH and carbonate ion concentration (runs DT-2, DT-3, DT-4 and DT-11) are illustrated in the plots of Fig. 2 and reported in Table 2. These plots show that, as one might expect (cf. Lüttge et al., 2003), the three r-planes dissolved approximately by the same amount after each tested experimental condition, displaying however up to 55% variation with respect to the mean value of the retreats measured on the same crystal. It is also evident that surface retreat rates decreased with increasing pH and total carbonate concentration, in agreement with the results of previous macroscopic studies (e.g., Chou et al., 1989; Pokrovsky and Schott, 2001). The reactivity of the c-plane varied more rapidly compared to the r-planes as a function of the fluid composition: c-plane retreat rates were apparently faster than r-plane rates under mildly acidic conditions (expt. DT-2, Fig. 2a) but became slower as pH and carbonate ion concentration increased (Fig. 2b and c). As shown in Fig. 2c, the c-plane dissolution at pH 9 was slower than the dissolution of the adjacent r-planes.

3D maps of unreacted and dissolved crystal faces permitted identification of the variation of dissolution fluxes over the entire surface of the analyzed crystal face and quantification of the face-specific total rates of dissolution. A reconstructed 3D image of the 4 faces of the crystal analyzed after the experiment DT-2A is shown in Fig. 3. The picture clearly shows the relief of the unreacted portion of
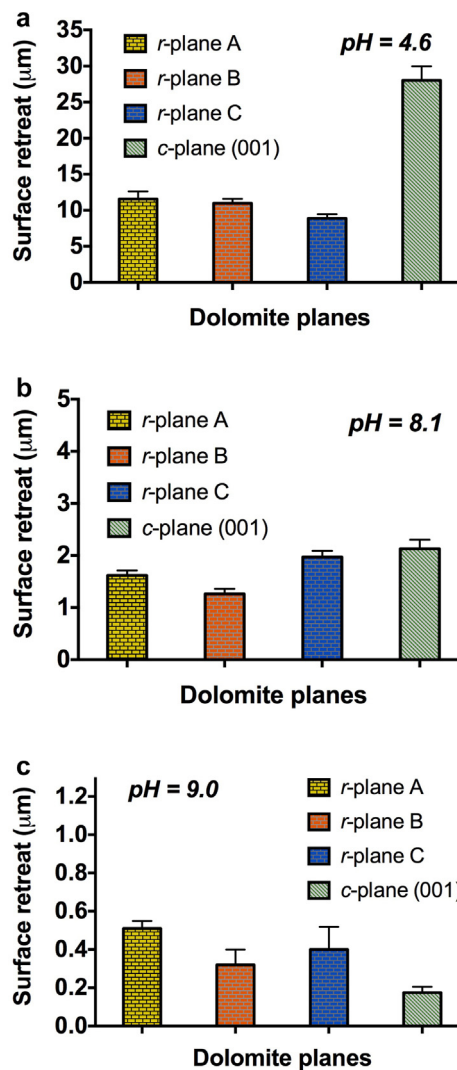

Fig. 2. Vertical surface retreats of four dolomite single-crystal polished faces as a function of pH and total carbon concentration (ΣCO_2) after 4–8 day-long experiments: (a) pH = 4.6, $\Sigma CO_2 < 10^{-4}$ M; (b) pH = 8.1, $\Sigma CO_2 = 0.001$ M; (c) pH = 9.0, $\Sigma CO_2 = 0.04$ M. Three faces are parallel to the $\{10\bar{1}4\}$ cleavage planes and designated as "r-planes" (A, B and C) and one perpendicular to the $[001]$ crystallographic direction and named "c-plane".

the faces that were protected with Viton (largest elevated area) and silicone glue masks. The surface distribution of the dissolution fluxes was obtained by a histogram analysis of the height distribution of the surface after reaction (cf. Fischer et al., 2012; Emmanuel, 2014). Rate spectra relative to single r-planes and c-planes of the crystals reacted at different pH conditions are represented in Fig. 4 and 5. It can be observed that: (i) the mean values of the data distributions reflect the dependence of dissolution rates on the aqueous fluid composition, with spectra located at lower rate values for increasing pH's; (ii) the variance of the data distribution tends to decrease with increasing pH values, reflecting the generally lower and more uniform reactivity of the surface at basic pH and high carbonate concentrations. The asymmetry exhibited by these spectra is related

Table 2
Summary of the average surface retreats and corresponding mean rates of dissolution for dolomite crystals at the studied conditions. All the experiments were conducted with the same fluid flow rate, equal to 0.5 ml/min, and the aqueous solutions in the reactor were mixed at a constant speed of 350 rpm. Note that mean r-plane and c-plane dissolution rates express the average value of measured retreat rates for these planes. Provided surface rate ranges refer to 90 % of the observed surface reaction distributions between slow- and fast- dissolving planes of the analyzed crystals.

Run #	Surface treatment	Outlet pH (50 °C)	Crystal Face retreats (µm)		Mean r-plane dissolution rate (mol/cm²/s)	Mean c-plane dissolution rate (mol/cm²/s)	Surface rate range (90% distribution) (mol/cm²/s)	Duration (days)
			r-planes	c-plane				
DT-1	Polished	4.52–4.82	7.00 ± 0.5	nd	3.3×10^{-11}[a]	nd	nd	3.9
DT-2A	Polished	4.64	11.58 ± 1.03 10.98 ± 0.62 8.88 ± 0.59	28.02 ± 1.97	4.5×10^{-11}	1.2×10^{-10}	$0.4–1.4 \times 10^{-10}$	4.2
DT-3	Polished	9.00	0.51 ± 0.04 0.32 ± 0.08 0.40 ± 0.119	0.18 ± 0.03	1.8×10^{-12}	7.6×10^{-13}	$0.5–3.4 \times 10^{-12}$	4.1
DT-4	Polished	8.12	1.62 ± 0.09 1.27 ± 0.10 1.97 ± 0.12	2.13 ± 0.17	3.6×10^{-12}	4.7×10^{-12}	$1.5–4.9 \times 10^{-12}$	8.0
DT-5	Polished	8.99	2.54 ± 0.11	nd	1.5×10^{-12}	nd	$1.3–2.3 \times 10^{-12}$	30
DT-5	Unpolished	8.99	0.87 ± 0.04	nd	5.2×10^{-13}	nd	$5.1–5.4 \times 10^{-13}$	30
DT-6	Polished	4.69–4.81	nd	4.22 ± 0.41	nd	7.5×10^{-11}	$6.2–10.5 \times 10^{-11}$	1.0
			nd	10.15 ± 0.22	nd	8.9×10^{-11}	$7.8–10.9 \times 10^{-11}$	2.0
			nd	17.83 ± 0.5	nd	8.8×10^{-11}	$8.6–9.1 \times 10^{-11}$	4.1
			nd	25.57 ± 0.7	nd	7.4×10^{-11}	nd	6.2
			nd	38.38 ± 1.4	nd	8.3×10^{-11}	nd	8.3
DT-7	Unpolished	4.79	8.79 ± 0.29	nd	4.1×10^{-11}	nd	$3.2–4.9 \times 10^{-11}$	3.8
DT-8	Polished	5.51	29.39 ± 1.62 23.31 ± 1.72 24.17 ± 0.51	82.92 ± 6.60	9.10×10^{-11}	2.95×10^{-10}	$0.80–3.3 \times 10^{-10}$	5.0
DT-8	Unpolished	5.51	8.47 ± 1.33	nd	3.0×10^{-11}	nd	$2.3–5.3 \times 10^{-11}$	5.0
DT-9	Polished	4.86	8.80 ± 0.53 15.27 ± 1.13	nd	5.30×10^{-11}	nd	$3.0–9.2 \times 10^{-11}$	4.0
DT-9	Unpolished	4.86	8.89 ± 0.18 15.93 ± 0.36	nd	5.47×10^{-11}	nd	$3.1–9.1 \times 10^{-11}$	4.0
DT-11	Polished	3.41	16.93 ± 0.50 16.49 ± 1.11 17.98 ± 0.54	30.90 ± 10.9	3.54×10^{-10}	6.38×10^{-10}	$2.7–6.6 \times 10^{-10}$	0.9

[a] Retreat rate deduced by linear interpolation of measured retreats as a function of time.
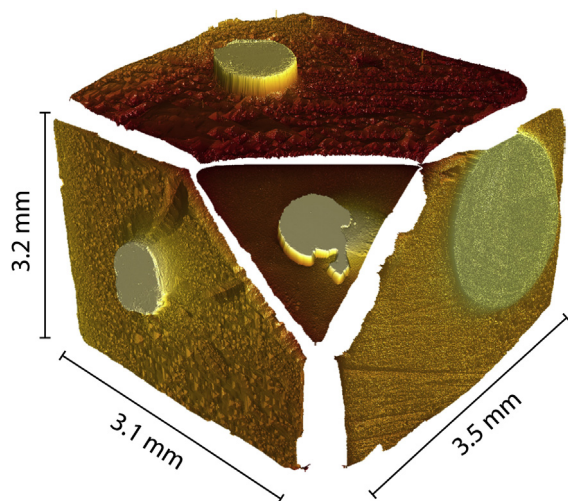
Fig. 3. 3D-reconstructed view of a dolomite crystal dissolved under acidic conditions (run DT-2A, pH = 4.6). The topographic images of each face were obtained by VSI measurements after the experiment. The crystal faces were polished and covered with a Viton disc and three silicone glue spots to maintain the unwetted reference surfaces required to measure the corresponding normal retreat of each face (see Fig. 1). The surface regions that were protected against dissolution are visible as rounded, elevated areas in the central portion of each face.

either to the presence of comparatively unreactive portions of the surface, such as wide terraces (Fig. 4b), or to the presence of particularly reactive sites represented by deep etch pits the development of which is more favorable under acidic conditions (Fig. 4a). Along with the spectra, the plots also report the corresponding mean values of each distribution, calculated by integration of the data of each spectrum and represented by a red vertical line. We can note that mean dissolution rates of r-planes decreased by a factor of 200 between pH 3.4 and pH 9.0, whereas if we look at the entire surface reaction distribution the dissolution rate of r-planes varied by about 600 times between these two pH extremes. An example of a rate spectrum of a c-plane is reported in Fig. 5. Rate spectra of c-planes were found to be generally more symmetrical in shape but showing an increasing variance of the rate distribution data with increasing reaction time as a consequence of developing topography and increasing roughness (see Section 3.3).

The comparison of the surface rate distribution relative to different r-planes allows a good estimate of the actual intrinsic variability of dolomite dissolution fluxes reacted under given conditions. Fig. 6 compares the rate spectra of two pairs of r-planes reacted at the same time at pH = 4.9. One pair of spectra (red color) corresponds to the cleavage planes of a polished crystal, whereas the other two spectra (blue color) refer to the r-planes of an unpolished crystal that underwent dissolution during the same experiment (run DT-9). The plot shows that equivalent faces of the same crystal display different distributions of dissolution fluxes and contribute to a wide variability in terms of dissolution rate, which spans over almost one order of magnitude but with a corresponding change of mean rate values by a factor of ~2. Apart from a slightly
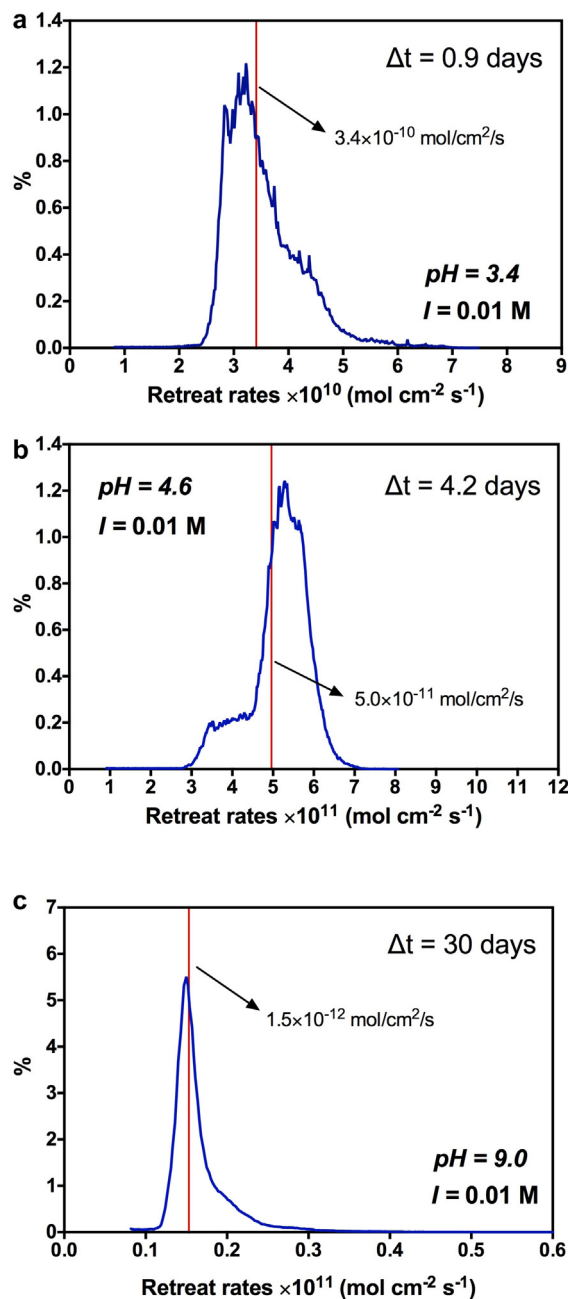

Fig. 4. Calculated rate spectra of dolomite r-planes obtained by surface analysis of VSI data for different pH conditions and reaction times, under constant ionic strength (0.01 M NaCl): (a) pH = 3.4, Δt = 0.9 days; (b) pH = 4.6, Δt = 4.2 days; (c) pH = 9.0, Δt = 30 days. On each plot is also reported the mean rate value, as obtained by integration of the data of the corresponding spectrum.

different shape of the spectra, no clear difference is evident between the dissolution behavior of polished and unpolished r-planes of the two crystals at acidic conditions. The comparison between polished and unpolished r-plane reactivities under basic conditions suggests instead that the polishing procedure enhanced appreciably the dissolution reaction. At pH = 9, mean retreat rates of unpolished r-planes were in fact about 3 times slower than those mea-
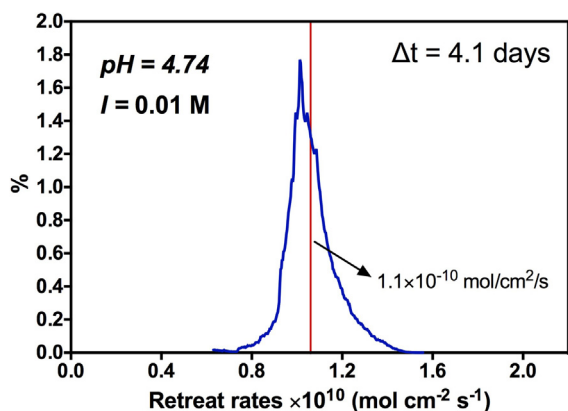
Fig. 5. Rate spectrum of a dolomite *c*-plane dissolved at 50 °C under acidic conditions (pH = 4.7) for 4 days. The red vertical line represents the mean value of the rate distribution. (For interpretation of the references to color, the reader is referred to the web version of this article.)
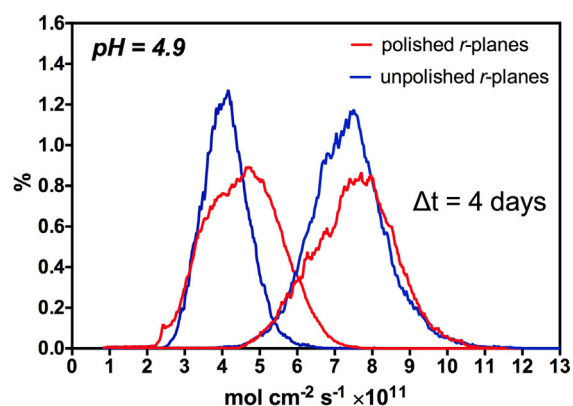

Fig. 6. Comparison between the rate spectra of two pairs of adjacent *r*-planes from two different dolomite crystals reacted under the same experimental conditions ($T = 50$ °C; pH = 4.9). One crystal was polished prior to the reaction (red data-lines) while the other one was dissolved without any surface treatment before the experiment (blue data-lines). Both crystals exhibit the same overall reactivity but an evident difference exists between the dissolution rate distributions of the two *r*-planes of each crystal, one face dissolving approximately two times faster than the other. (For interpretation of the references to color, the reader is referred to the web version of this article.)

sured on the corresponding polished surfaces (see Table 2). This result is consistent with the observations of Schott et al. (1989), who reported a larger increase of calcite dissolution rates with strain in more alkaline solutions. However, the observed effects of polishing on the rates are also related to the limited extent of the reaction, which took place within the restricted crystal volume affected by the mechanical treatment (see Section 4.1).

It is interesting to note that the same enhancement of the dissolution reaction by surface polishing reported at pH = 9 was also observed for the experiment conducted at pH 5.5 in acetate-bearing solutions (run DT-8, Table 2). As observed by Schott et al. (1989), such rate enhancement becomes generally significant when the dissolution reaction

is no longer transport-limited but controlled by surface hydrolysis. Dolomite dissolution reaction becomes pH-independent and promoted by the hydration of surface metal sites at pH > 5 (Pokrovsky and Schott, 2001; Schott et al., 2009).

In Table 2 we provide some estimates of the dissolution rate variability of dolomite surfaces based on the rate distribution (rate spectra) observed for the crystals analyzed after the reported experiments. The two extremes of each rate range refer to 90% of the spectral distribution with respect to the analyzed planes. It should be noted that the reported rate interval is narrow when only one plane was investigated: rates vary by a factor of 1.1–2.3 between the two extremes. When two, three, or four planes were examined, the resulting ratio between the two extremes of the rate range varies between 2.4 and 6.8. Given their different intrinsic reactivity, where both *r*-planes and *c*-planes are considered, the rate variation is larger.

3.2. Topographic characterization and morphologic evolution of reacted surfaces

The microtopography of reacted dolomite surfaces was characterized by combining VSI and AFM techniques to achieve a more accurate description of the most representative morphological features under the studied conditions. We will first describe the surface microtopography of the *r*-planes, under acid and basic pH conditions, and then the main morphologic features characterizing the dissolved *c*-planes.

The principal topographic features which characterize the *r*-planes under the acidic conditions here considered ($3.4 < $ pH $ < 5.0$) are illustrated in Fig. 7. Dissolution of cleavage planes is led by the formation of typical pseudo-rhombic etch pits, the size of which was observed to vary as a function of the fluid chemical composition and the reaction time. In the range of pH 3.4–3.5 and after 1 day of reaction (run DT-11), the etch pit size was observed to vary between 75 and 180 µm, whereas their depth was typically between 1.7 and 12.5 µm. For a longer exposure time (3.2 days, run DT-10) the surface was instead dominated by fewer but much larger etch pits having dimensions that varied between 450 and 500 µm and an average depth of about 9 µm. At these pH conditions the pit morphology was also characterized by a slight rounding of the obtuse steps (Fig. 7a), which can be attributed to a partial control by diffusion of the dissolution reaction (cf. De Giudici, 2002). Smaller dimensions characterized the dolomite etch pits that developed at pH of 4.6–4.9 after 4 days of exposure to the fluid (Fig. 7b): the quasi-rhombic etch pits showed horizontal dimensions between 30 and 150 µm with few pits reaching sizes of about 200 µm. Those pits displayed characteristic depths of 0.5 to 3 µm but reached up to 6 µm in few cases. For increasing time of reaction an evolution towards larger dimensions of dissolution pits was again observed. The same dolomite crystal reacted for 4 days (run DT-2) was dissolved in the same solution for two successive time intervals of 5 days (DT-2B–C). Pit size range increased first to 95–235 µm and then to 160–430 µm after the second step of dissolution, while pit depth range
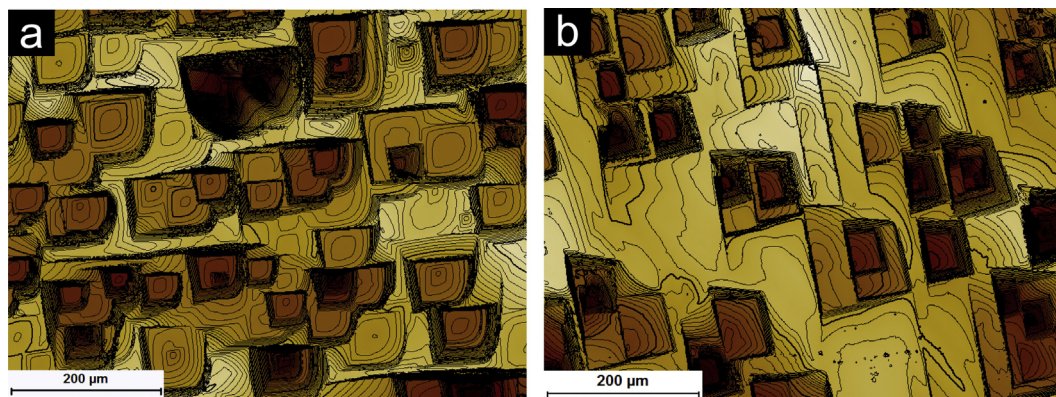
Fig. 7. Details of dissolution etch-pit morphology, size and distribution on the cleavage *r*-planes of dolomite at acidic conditions. a) Etch pits formed after 1 day of reaction at pH = 3.4; b) etch pits formed after 4 days of reaction at pH = 4.6. To better render the representation of surface micro-topography, contour lines with 100 nm vertical interdistance were added to both VSI images.

increased to 1.5–9.1 μm and remained essentially unchanged after the second dissolution period. No evident changes in geometry and density of dissolution pits were observed between initially polished and unpolished dolomite crystals under acidic conditions.

Remarkable changes in surface topography were found when dolomite crystals were dissolved at basic conditions. To illustrate the effect of the fluid composition on surface topography, we will limit our analysis to the experiment conducted at pH 9 for 30 days (run DT-5). Two dolomite crystals were used in this experiment, one polished on 3 *r*-planes and a *c*-plane, the other one unpolished and protected with masks only on the natural cleaved *r*-planes. Both samples were characterized by the development of abundant etch pits that exhibited a rounded shape in correspondence of the corner region between the two obtuse steps (Fig. 8a). This morphology can be attributed to the inhibiting effect of the high carbonate ion concentration in solutions ($[CO_3^{2-}] \approx 0.3$ mM). The same effect was in fact observed by Lea et al. (2001) when studying calcite dissolution in CO_3^{2-}-rich aqueous solutions ($[CO_3^{2-}]$ varying between 0.15 and 0.9 mM). This generation of etch pits showed horizontal dimensions that ranged between 15 and 40 μm and depths of 0.1–1.5 μm on the polished surfaces, whereas pits displayed relatively larger dimensions on the *r*-planes of the unpolished sample, being between 20 and 80 μm in width and varying between 0.4 and 3 μm in depth. A second generation of shallower pits was also distinguishable on the polished *r*-planes. These pits had an average size of 2–6 μm and were between 60 and 150 nm deep (Fig. 8b). The most striking aspect that distinguished the polished *r*-planes from the corresponding unpolished surfaces was the development of linear features that crossed the surface of the polished *r*-planes, which were the result of scratches and surface damage generated by the polishing procedure but were not clearly visible on the freshly polished crystal surfaces. The following etching process amplified the effects of the surface treatment suggesting that subsurface damage could be produced by small fragments of dolomite breaking from the edges and rolling under the crystal surface during the polishing. These fea-

tures appeared like trenches 15–80 μm wide and 0.3–1.5 μm deep, consisting of linear arrays of pits (Fig. 8c). The development of these linear features was also evident on the polished crystal reacted for 4 days at the same conditions (run DT-3).

The surface topography of the reacted triangular *c*-plane is quite different from the adjacent *r*-planes described above. Under acidic conditions the dissolution of this surface results in the development of pyramidal features, with no evidence of etch pit formation accommodating the dissolution reaction (Fig. 9). On the contrary, under basic conditions (pH 9, run DT-5) the surface topography was characterized by the formation of triangular etch pits, which were analogous to those observed by Smith et al. (2013) on the equivalent crystallographic plane of calcite dissolved at various degrees of fluid saturation. Such pits could not be distinguished on the {0001} plane surface after only a few days of reaction but were clearly visible on the dolomite crystal reacted for 30 days (Fig. 10).

3.3. Rate variation and surface topography evolution as a function of time: $\{10\bar{1}4\}$ vs. $\{0001\}$

Measurements of surface retreat rates as a function of time were conducted at pH of ∼4.7 both for an unpolished *r*-plane and a polished *c*-plane by masking the same surface region and measuring the height difference with respect to the underlying topography at different time steps (Fig. 11). The surface normal retreat of both planes showed an approximately linear dependence on time. The observed trends of *r*- and *c*-plane retreat rates can be compared with the corresponding evolution of the surface roughness during the course of the reaction. Plots of the evolution of the root square mean (RMS) roughness (R_q) measured for an *r*-plane and a *c*-plane under the investigated conditions are reported in Fig. 12. R_q values were obtained for fields of view of 692 × 518 μm and 105 × 140 μm for the *r*-plane and the *c*-plane, respectively. It can be observed that, while the increase of RMS roughness is linear for the *r*-plane, the progress of this parameter follows an exponential increase for the *c*-plane as a function of time,
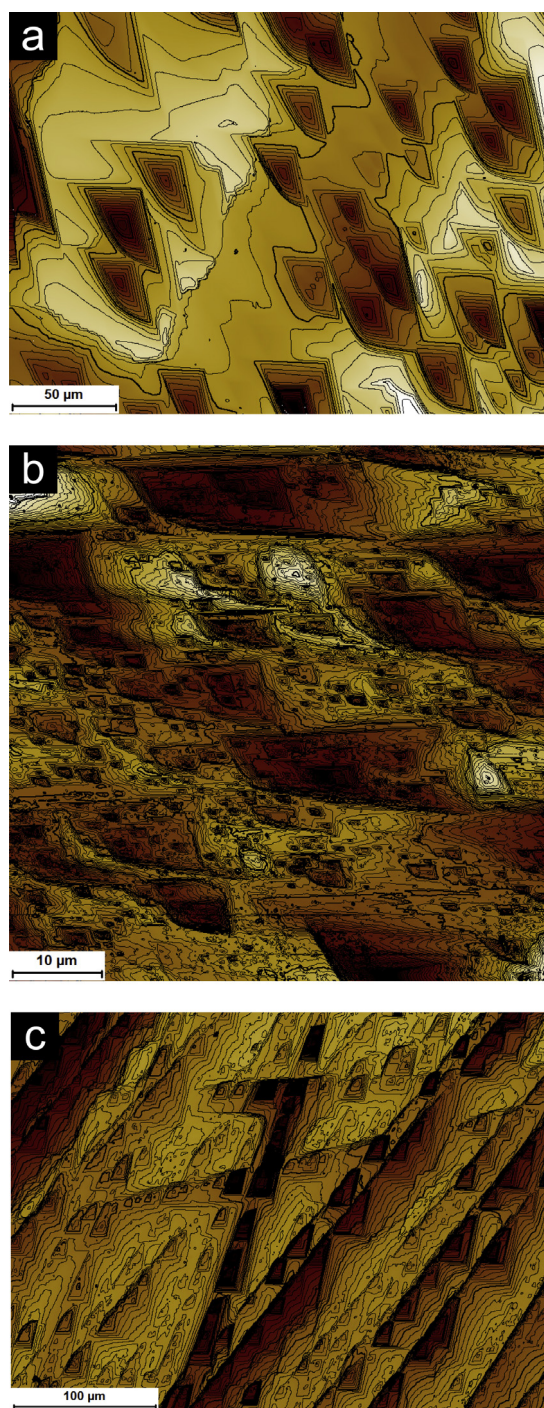
Fig. 8. Typical surface topography and etch pit morphology of dolomite r-planes reacted under basic conditions and high carbonate ion concentration (pH = 9; $[CO_3^{2-}] = 0.3$ mM). As in Fig. 7, contour lines were added to the images to better visualize the morphology and depth of the represented features. (a) Dissolution under high $[CO_3^{2-}]$ results in the formation of etch pits with rounded shape on the obtuse step side (VSI image of an unpolished r-plane). (b) AFM image showing the presence of two different generation of etch pits on the polished surface of an r-plane. (c) VSI image showing how triangular-rounded shaped etch pits are concentrated along linear features inherited by the polishing procedure. Contour line vertical interdistance is 100 nm in (a), 10 nm in (b) and 75 nm in (c).

although R_q varied by less than 1 μm in the latter case. This indicates that the progress of the dissolution reaction brought about a relative decrease of surface reactivity due to the development of a progressively less reactive surface morphology (see Section 4.2).

3.4. Fluid chemical data

The composition of the aqueous solution reacting with the dolomite crystals was analyzed for Ca and Mg concentrations during the progress of the experiments. In the case of the runs conducted at pH 8 and 9, because of the slow rates of dissolution and the very high solution volume to dolomite surface area ratio, Ca and Mg concentrations were below the detection limit for ICP-OES, so that we could not follow the chemical evolution of the fluid at these conditions. The composition of the aqueous solution could be monitored during the experiments conducted under acidic conditions (pH ≤ 5.5). The analytical data for these conditions show that the Ca/Mg concentration ratio in the solution increases with decreasing pH, varying from 0.95 at pH 5.5 (run DT-8) to 1.12 at pH 3.4 (run DT-11), whereas the Ca/Mg ratio of the solid equals 1.01. These data are consistent with a preferential departure of Ca from the mineral surface and the formation of a Mg-rich surface layer at pH < 5.0 (cf. Pokrovsky and Schott, 2001; Urosevic et al., 2012). The evolution of the Ca and Mg concentrations during the experiment DT-2A–C performed at pH of ~4.7 is illustrated in Fig. 13. This experiment was carried out in three separate steps, interrupting the reaction at 4 and 5 day intervals to look at the morphologic evolution of the crystal surfaces during the reaction. The plot of Fig. 13 shows that the concentration of the two elements reached a steady state after a period of 60–90 h (first step of reaction) and remained relatively constant during the following 200 h (second and third steps of reaction) but showing a slight increase after 300 h, right before the end of the experiment. This apparent increase may be related to the change of reactive surface area of the crystal after the first several days of dissolution (see discussion below). Element concentrations and corresponding saturation ratios of the aqueous solution with respect to dolomite and calcite are listed in Table 3.

4. DISCUSSION

The results presented here show how the dissolution behavior of dolomite surfaces varies not only as a function of changing chemical conditions but is also intrinsically related to the heterogeneous distribution of surface defects and the inherited surface morphology resulting from sample treatment and reaction history (cf. Arvidson and Lüttge, 2010). In this regard we observed how the surface damage generated by mechanical polishing enhanced the reactivity of the crystals at near neutral pH and conditions otherwise relatively unfavorable to dissolution (basic pH and carbonate-rich fluids). The morphologic progression of dissolving dolomite surfaces varied as a function of aqueous solution composition and controlled in its turn the rates of the overall dissolution reaction. Understanding the
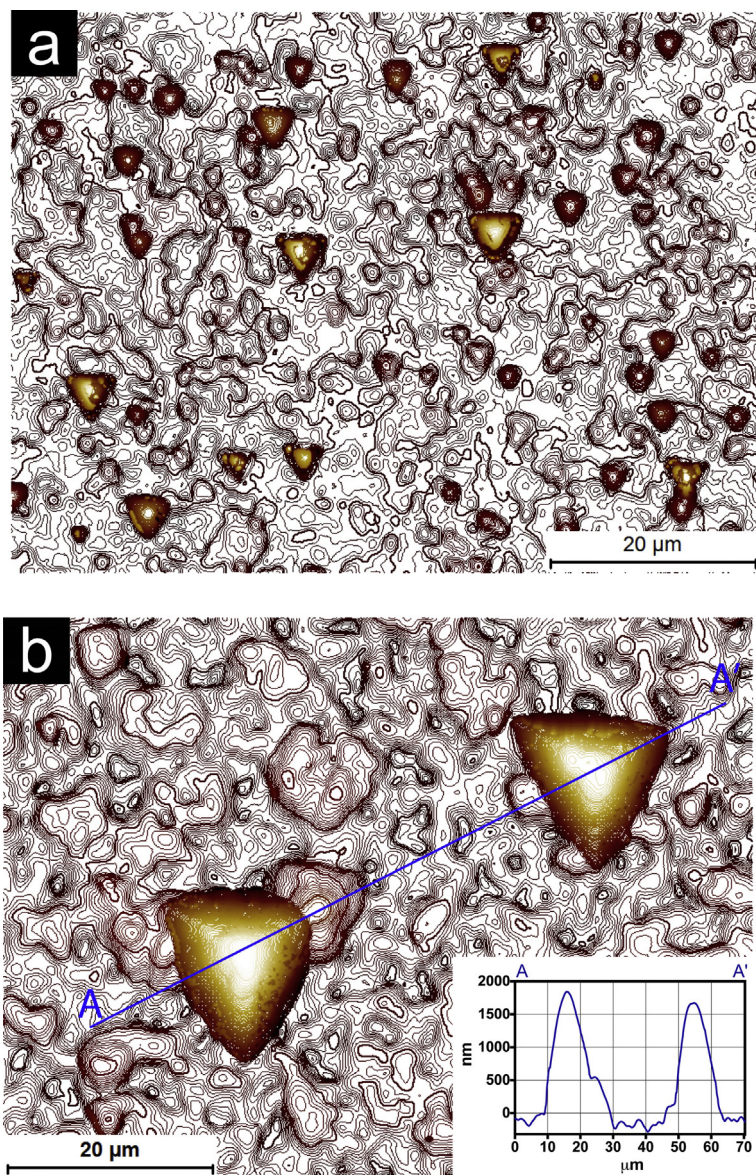
Fig. 9. *c*-plane surface morphology of dolomite after 48 h (a) and 144 h (b) of reaction under acidic conditions (pH = 4.7, run DT-6). Dissolution of the *c*-plane at these conditions brings about the development of pyramidal features the density and size of which increase as a function of the reaction time and lead to a less reactive surface. The vertical interdistance of the drawn contour lines is 25 nm.

effects of different parameters on dolomite surface topography and reactivity is thus crucial to model the dissolution behavior of this mineral under a wide range of conditions. In the following subsections we discuss our experimental results in relation to the investigated parameters (mechanical polishing, fluid chemistry, surface orientation and reaction time) to provide a more comprehensive description of dolomite dissolution rates and their intrinsic variability.

4.1. Influence of mechanical polishing on surface topography and measured retreat rates

Pretreatment of dolomite surfaces did not have any apparent effect on measured dissolution rates under the tested acidic conditions (pH ≤ 4.9). Under these conditions

an increase of the dissolution rates for polished surfaces can be expected but it is generally transitory and limited to the early stages of the reaction, where a relative increase of surface area combines with decreasing surface energy due to dislocation cores opening and expanding (Schott et al., 1989; Lasaga and Lüttge, 2001). Because the number of active sites on the mineral surface largely exceeds the density of defects and dislocations even in strained samples, the dissolution behavior of polished crystals under acidic conditions will be negligibly affected by the increase of the defect density and the presence of various surface artifacts (cf. Lüttge, 2005). This is confirmed by the comparison of couples of polished and unpolished crystal faces reacted under the same conditions at pH 4.9 (Fig. 6), the surface normal retreats and rate distributions of which
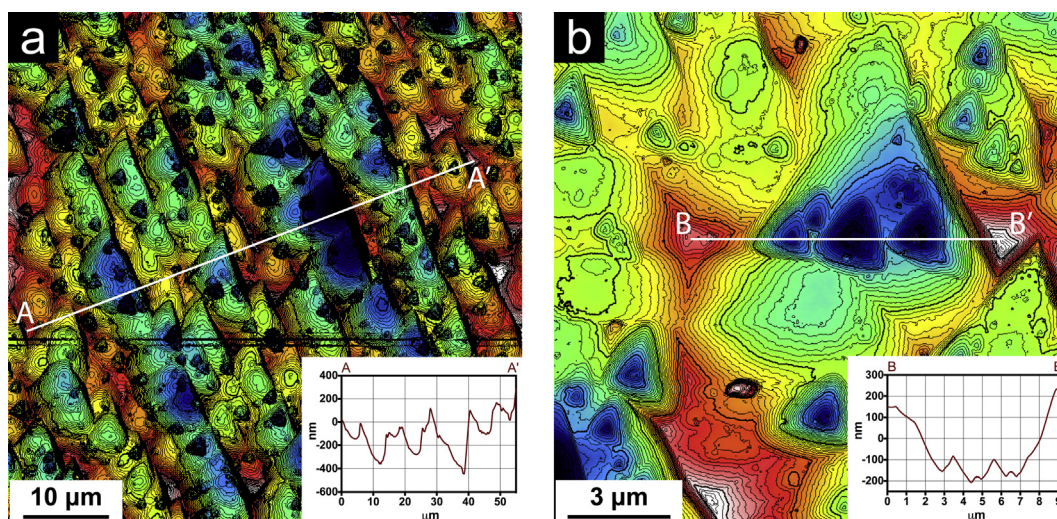
Fig. 10. AFM images of dolomite *c*-plane surface morphology developed after 30 days of reaction under basic conditions (pH = 9.0). Different from acidic conditions, the surface shows the formation of triangular etch pits. Note that (b) shows a detail of the surface represented in (a). Contour line vertical interdistance is 20 nm on both images.

show negligible differences. Nonetheless, the different rate distribution between the two *r*-planes of each crystal is clear and could not be related to any distinctive feature that would explain it. Therefore, we simply assume that the observed difference in rate distributions is an expression of the intrinsic variation of surface energy that characterizes dolomite cleavage planes. On the contrary, at alkaline pH's and high carbonate ion activities (runs DT-3, DT-5) the increased density of surface defects generated by mechanical polishing corresponds to a large increase in the concentration of dissolution-active sites compared to a smooth or unpolished surface (cf. Pokrovsky and Schott, 2001; Duckworth and Martin, 2003), resulting in enhanced dissolution rates. The influence of polishing on the reactivity of dolomite is clearly exhibited by the morphology of the *r*-planes reacted at pH 9.0, where dissolution took place preferentially along scratches and microfractures inherited by the surface treatment (Fig. 8b and c). These features locally increased the energy of the surface by providing preferential sites for the nucleation of etch pits and their subsequent expansion, which constitutes the fundamental mechanism driving the normal retreat of the surface under those conditions (cf. Lasaga and Lüttge, 2001).

Similarly, the increased density of surface defects explains the faster rates of dissolution observed for polished crystals in acetate-bearing solutions at pH = 5.5. It should be noted that no clear effect of acetate ions on the rates of both polished and unpolished surfaces could be observed at the concentration level used in this study (2.5 mM). This ligand can catalyze carbonate mineral dissolution at concentrations higher than 10 mM but its effects are generally less important compared to other organic ligands (Pokrovsky and Schott, 2001; Pokrovsky et al., 2009).

According to the measured vertical retreats and corresponding surface topography, it is evident that the adopted polishing method affected the crystal structure and its reactivity to a depth of several micrometers below the surface, which is consistent with studies of near surface damage generated by mechanical polishing of various crystalline materials (Lucca et al., 2006; Klopfstein and Lucca, 2011). This fact implies that, if the same conditions are maintained, the observed surface topography and the increased retreat rates represent transient non-steady state conditions towards a smoother topography and slower rates of dissolution, which will be attained after the extent of surface retreat becomes larger than the thickness of the crystal affected by damage due to sample treatment. The higher dissolution rates obtained from the analysis of polished crystals at pH > 5 are thus related to the removal of a volume of material that was affected by the polishing procedure and are not representative of steady state conditions.

4.2. Morphologic evolution of c-planes and r-planes as a function of pH and reaction time

Remarkable differences in mean rates and rate spatial distribution were evident by the comparison of dolomite *r*-plane and *c*-plane surface topography as a function of time and fluid composition. As observed above, the *c*-plane dissolved 2–3 times faster than the *r*-plane at acidic conditions but slower in basic and CO_3-rich fluids (Fig. 2). However, the rate spectra obtained by analysis of the surface before and after a few days of dissolution revealed that *r*-planes were generally characterized by a wider variability in rate distribution than *c*-planes, particularly at acidic pH's, where the heterogeneous distribution of surface energy was manifested in the asymmetric shape of the rate spectra and the corresponding frequency of highly reactive sites (deep etch-pits) versus comparatively slow dissolving regions (e.g., wide flat terraces between major etch-pit arrangements; see Fig. 4b). Although the surface area of
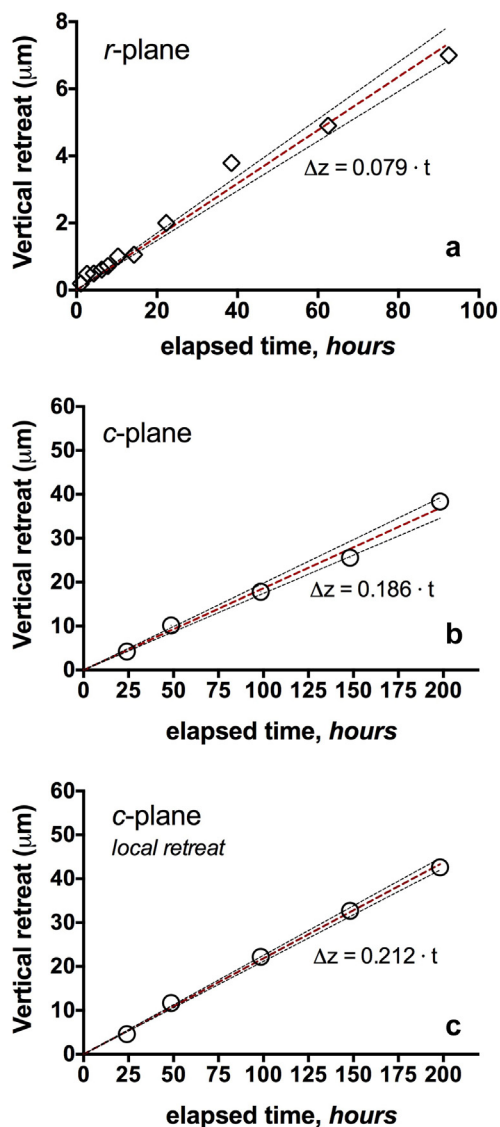
Fig. 11. Vertical retreat of dolomite surfaces as a function of reaction time. a) Total retreat variation of an *r*-plane at pH 4.7 over a 4 days period. b) Total rate variation of a *c*-plane at pH 4.7 over an 8 days period. c) Local retreat variation of the same *c*-plane of (b) relative to an area not affected by the formation of pyramidal features. Dashed lines drawn through the symbols represent a linear least square fit of the data with the 95% confidence interval (thin black dotted lines).

form of trigonal carbonates (F faces). On the contrary, the *c*-planes do not contain any PBC direction and are kinked (K) faces, which, as a result, are very unstable. Therefore, the higher reactivity of the *c*-plane under acidic conditions is not surprising if one considers its highly kinked nature and consequent instability compared to the cleavage plane. However, the morphologic evolution of this plane indicates that its reactivity might decrease progressively as a function of time in the acid pH range, as shown by the formation and growth of pyramidal protrusions mimicking the intersection of the adjacent dolomite cleavage planes. The growing emergence of such features was responsible for the exponential increase of surface roughness (R_q) but did not impact considerably the retreat rates measured under these conditions (Fig. 11b), probably because the increase of surface roughness was limited to few hundreds nm (Fig. 12b). Nevertheless, if we consider the vertical retreat of a restricted region not affected by the formation of those features (Fig. 11c), we observe that the retreat rates were slightly faster compared to the retreats measured on the entire surface. This suggests that, if the reaction was protracted for a longer time, the average retreat rate of this plane will eventually decrease while surface roughness will keep increasing as a consequence of the further development of the observed surface microtopography. An inverse relation between total retreat rates and surface roughness was reported by Godinho et al. (2014) when dissolving different faces of fluorite crystals and is consistent with the evolution of the surface towards a more stable (low-energy) topography.

The elementary mechanism leading to the formation of the observed microscopic pyramids on the *c*-plane is not clear because we could not distinguish any regular morphologic pattern connecting the emergence of such features on the *c*-plane surface. Formation by a (re-) precipitation mechanism can be excluded given the highly undersaturated conditions of the aqueous solution (cf. Table 3) and considering that the relative height of these protrusions did not increase with time compared to the unreacted reference surface. Regardless of the microscopic mechanisms, the observed morphological progression of the *c*-plane (Fig. 9) suggests that the {0001} surface might macroscopically evolve into a {10$\bar{1}$4} form on the long term, as the pyramidal protrusions grow in size and total retreat rates decrease to approach those measured on the *r*-plane. Directions and surface angles of the microfacets bounding the pyramidal features developed on the {0001} also seem compatible with *r*-planes. Such evolution becomes instead more unlikely if we look at the topography developed by the *c*-plane at pH 9. Under these conditions the surface is dominated by the presence of small-sized triangular pits with wall inclination close to the {10$\bar{1}$4} orientation (Fig.10). Although we do not have a time sequence showing the morphologic progression of this plane, we can argue that, in analogy with the mechanisms proposed by Smith et al. (2013) for calcite *c*-plane reactivity, this surface will eventually maintain its {0001} macroscopic form. Irrespective of the long-term three-dimensional evolution of dolomite crystals (see next section) the evident divergence of *c*-plane dissolution behavior between acidic and basic con-
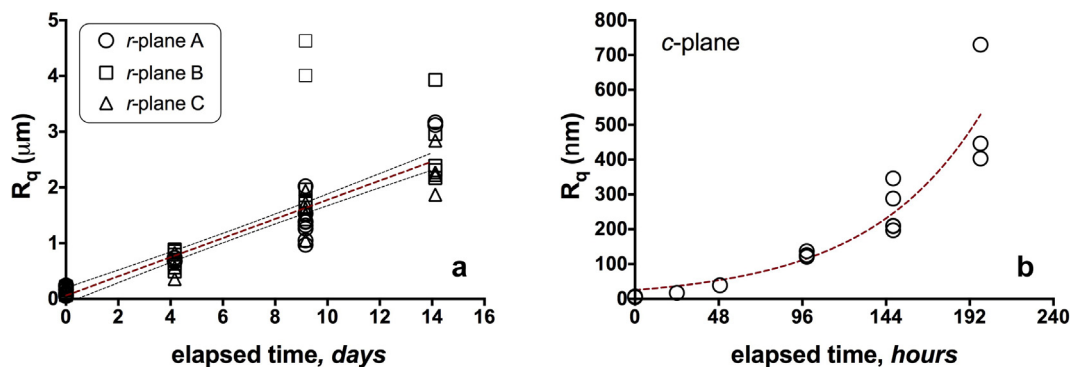
analyzed *c*-planes was between 3 and 6 times smaller than the *r*-planes, such size difference does not explain the fundamentally distinct surface reaction distribution, which stems from different reaction mechanisms. The different dissolution behavior of the two planes can be compared by considering the periodic bond chain (PBC) model of Hartman and Perdok (1955), which relates the nature and reactivity of different faces to the number of the continuous chains of strong bonds they contain. Dolomite *r*-planes are characterized by three non-parallel PBCs (Fouke and Reeder, 1992; Paquette and Reeder, 1995) and constitute the most stable

Fig. 12. RMS roughness (R_q) evolution of r-plane (a) and c-plane (b) surfaces as a function of reaction time at mildly acidic pH ($4.6 \leq pH \leq 4.8$). FOV is of 692×518 μm for the r-planes and 105×140 μm for the c-plane. Refer to Fig. 11 for the corresponding variation of total retreat rates. Dashed lines drawn through the symbols represent a fit to the data to illustrate the linear and exponential increase of R_q with time for r-planes and c-plane, respectively.
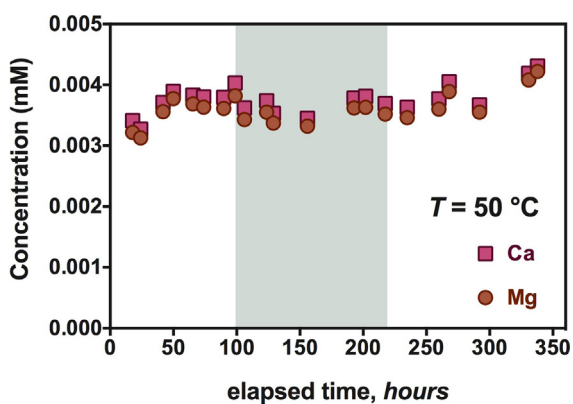

Fig. 13. Variation of Mg and Ca concentration with time for the experiment conducted in three separate reaction steps (DT-2A–C) under acidic conditions (pH = 4.7). Each reaction step is delimited by a different background color on the plot area. Concentrations reach a steady state during the first step of the reaction and keep it through the successive stage of dissolution but they seem to increase near the end of the 3rd reaction step, indicating a possible increase of the reactive surface area of the dolomite crystal.

ditions favors, in both cases, the development of a more stable microtopography, but suggest that the different microscopic features observed on this plane (triangular protrusion vs. triangular pits) are the result of surface dynamic processes whose sensitivity to changed chemical conditions is higher than on contiguous r-planes. As a consequence, when measured c-plane retreat rates are faster than r-planes pyramidal protrusions are formed, whereas the slower dissolution of the c-plane at basic conditions (and high dissolved inorganic carbon concentrations) leads to the development of triangular etch pits, which likely control the overall retreat of the surface.

The morphologic study of the r-plane showed that shape, size and spatial distribution of the etch pits controlling the dissolution process is strongly influenced by the pH of the aqueous solution. As it was previously observed by Orton and Unwin (1993), dolomite dissolution at room T can also exhibit a highly anisotropic character with respect to the fluid-flow conditions at pH as low as 3–4, where etch-pit geometry and distribution are controlled by the rate of solute transport. Evidence of rate dependence on mass-transport was observed at the low pH end of this experimental study (pH = 3.4), where etch pits displayed an evident rounding of obtuse step corners (Fig. 7a). In that regard it is worth considering that the increase of pH at the dolomite/fluid interface due to transport control was presumably very small (cf. Gautelier et al., 1999) and thus unable to affect considerably the saturation state of the interfacial fluid compared to the bulk solution. We do not have any clear evidence of diffusion-limited rates at the higher pH's investigated in this study ($4.5 < pH < 5.0$), but a mixed control by surface reaction and solute transport cannot be excluded a priori in the acidic to near neutral pH region (cf. Gautelier et al., 1999). Furthermore, the evolution of the cleavage surface at mildly acidic conditions (pH = 4.7) is characterized by the progressive expansion and deepening of a few etch pits, which is consistent with the growth behavior described by Lüttge et al. (2003) at pH 3 and 25 °C for the same dolomite planes. As shown in Fig. 12a the growth of those etch pits is accompanied by a relatively constant increase in surface roughness, which suggests that, at least at these conditions, a morphological steady state may not be reached with time at the surface of dolomite r-planes. The attainment of such condition could be in fact a quite fortuitous event and would require a discontinuous character of the etch pit nucleation process (MacInnis and Brantley, 1992). Nonetheless, the surface-normal retreat of the r-plane as function of time remains essentially constant (Fig. 11a) despite the observed increase in surface roughness, suggesting that the apparent increase of surface area is balanced by an increasing proportion of surface features characterized by a lower reactivity (cf. Godinho et al., 2014) such as the steep walls of expanding etch pits, where the formation of step bunches and macrosteps by interstep interaction (Jordan and Rammensee, 1996; Smith et al., 2013) could lead to a significant reduction of local dissolution rates. In other words, the relatively uniform and constant vertical retreat of the surface is primarily controlled by the movement of the steps present at the boundaries of widening,

Table 3
Aqueous solution concentration change in Ca and Mg during the experiment DT2A–C, conducted at pH 4.7 and 50 °C at a constant flow rate of 0.5 ml/min. Refer to Fig. 13 for the plot of Ca an Mg concentration as function of time. SI defines the saturation index of the aqueous solution with respect to dolomite (Dol) and calcite (Cc).

|	Sample	Elapsed time (hours)	pH (50°C)	Ca (mM)	Mg (mM)	Ca/Mg	SI(Dol)	SI(Cc)
1st step	DT-2A-1	17.7	4.63	3.41E−03	3.22E−03	1.06	−16.6	−8.9
	DT-2A-2	24.1	4.62	3.27E−03	3.13E−03	1.05	−16.7	−9.0
	DT-2A-3	41.7	4.67	3.71E−03	3.56E−03	1.04	−16.4	−8.8
	DT-2A-4	49.9	4.64	3.89E−03	3.77E−03	1.03	−16.4	−8.9
	DT-2A-5	65.3	4.67	3.83E−03	3.69E−03	1.04	−16.3	−8.8
	DT-2A-6	73.9	4.65	3.80E−03	3.63E−03	1.05	−16.4	−8.8
	DT-2A-7	89.8	4.63	3.79E−03	3.61E−03	1.05	−16.5	−8.9
	DT-2A-8	98.8	4.64	4.03E−03	3.82E−03	1.06	−16.4	−8.8
2nd step	DT-2B-1	106.1	4.65	3.62E−03	3.43E−03	1.06	−16.5	−8.9
	DT-2B-2	123.7	4.65	3.74E−03	3.55E−03	1.05	−16.4	−8.9
	DT-2B-3	129.0	4.72	3.53E−03	3.37E−03	1.05	−16.2	−8.7
	DT-2B-4	156.0	4.62	3.45E−03	3.32E−03	1.04	−16.6	−9.0
	DT-2B-5	192.8	4.69	3.78E−03	3.62E−03	1.05	−16.3	−8.8
	DT-2B-6	202.0	4.67	3.81E−03	3.63E−03	1.05	−16.3	−8.8
	DT-2B-7	217.5	4.72	3.69E−03	3.52E−03	1.05	−16.2	−8.7
3rd step	DT-2C-1	234.9	4.64	3.63E−03	3.46E−03	1.05	−16.5	−8.9
	DT-2C-2	259.9	4.73	3.77E−03	3.60E−03	1.05	−16.1	−8.7
	DT-2C-3	267.9	4.63	4.05E−03	3.89E−03	1.04	−16.4	−8.9
	DT-2C-4	292.0	4.65	3.67E−03	3.55E−03	1.04	−16.4	−8.9
	DT-2C-5	330.9	4.76	4.19E−03	4.08E−03	1.03	−15.9	−8.6
	DT-2C-6	337.9	4.71	4.31E−03	4.22E−03	1.02	−16.1	−8.7
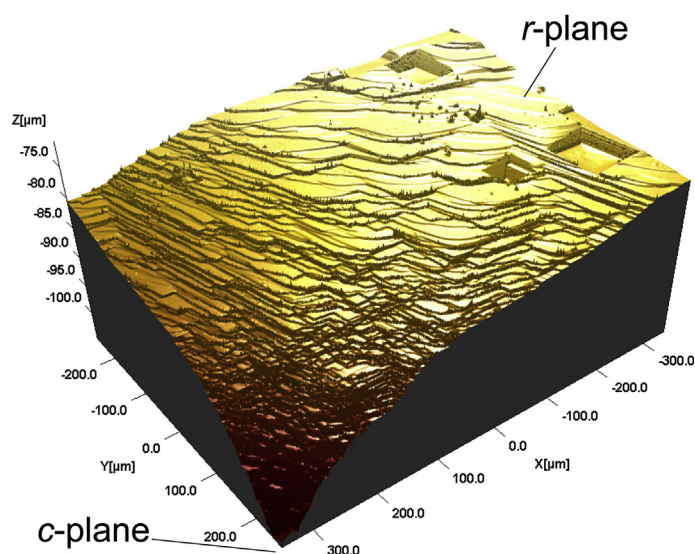
Fig. 14. 3D-plot of dolomite crystal topography at the edge region between *r*-plane and *c*-plane after 9 days of reaction at pH 4.7 (runs DT-2A and DT-2B). VSI data show how, under acidic to mildly acidic conditions, the density of steps and kinks at edges and corners increases dramatically with respect to the relatively smooth surfaces of cleavage planes, whose retreat and topographic evolution are conventionally used for rate determinations. The contribution of edge and corner regions to the overall dissolution rate is not taken into account by common surface retreat measurements and in-situ observations but can explain some of the discrepancies existing between single-face derived rates and traditional bulk fluid measurements.

coalescing and deepening etch pits (Lasaga and Lüttge, 2001; Lüttge et al., 2003), such that the measured increase of surface roughness translates into a marginal impact on the resulting surface retreat rates, which remain approximately constant.

4.3. The unknown contribution of crystal edges and corners to dissolution rates

In this study we quantified the dissolution rates of different surfaces of dolomite single crystals by providing direct

measurements of vertical surface retreat rates and illustrating the heterogeneous distribution of the dissolution fluxes on the reacted surfaces through time. However accurate this approach can be, compared to other indirect measurements of mineral dissolution rates, it always deals with the relatively smooth surfaces of large single crystal faces without taking into account the corresponding contribution of edge and corner regions to the overall reactivity of the mineral. As pointed out by Arvidson et al. (2003), the absence of such quantitative information may be at the origin of some of the discrepancies between rates derived from AFM and VSI studies compared to bulk dissolution rates obtained from mineral powders. The presence of a high density of steps and kinks at the edges and corners of mineral grains will result in bulk dissolution rates that are higher than those derived by the kinematic study of crystal faces characterized by a relatively smooth topography, especially when the rate contribution from those regions is higher than their contribution to the total surface area, an effect that will be amplified for decreasing size of mineral grains (Arvidson et al., 2003, 2015; Fischer et al., 2012). Lüttge et al. (2003) observed that the missing contribution of crystal edges to the calculation of mean rates could explain the lower rates of dolomite dissolution measured at pH 3 compared to the rates determined by bulk dissolution experiments. The contribution from edges and corners of dolomite single crystals seems very important also under the mildly acidic pH's investigated in this study. Fig. 14 shows a 3D image of the edge region between an r-plane and a c-plane of a dolomite crystal reacted at pH = 4.7 for 9 days at 50 °C (expt. DT-2). The density of steps and kink sites is much higher than that observed on the adjoining cleavage planes. In addition, the extension of the edge regions between r-planes and c-plane and contiguous r-planes was observed to increase over the course of the reaction to the detriment of the surface area of those planes, suggesting an increasing contribution of highly reactive edge and corner regions to the overall dissolution rate. Such morphologic evolution of the crystal corresponds to a scenario in which steady acidic conditions lead to an overall increasing instability of the surface and a dramatic change of crystal morphology. Such morphologic evolution might explain the visible increase of Ca and Mg concentration in the fluid recorded for this experiment after 300 h of reaction, even though such correspondence is actually difficult to resolve (Arvidson et al., 2015).

The reactivity of corners and edges of single crystals should be considered carefully also under basic pH as well as at near equilibrium conditions, where the reactivity of the interior part of a crystal face might be significantly reduced relative to the borders. If such condition holds, the edge of the crystals will be the main source of steps moving over the surface and driving the dissolution process while etch pit nucleation at dislocations and point defects remains comparatively unfavorable. In this case, however, the edge regions are likely to become dominated by merged steps (macrosteps) formed by step-step interactions and step pinning processes (cf. Bonzel, 2003; Smith et al., 2013). Because the velocities of macrosteps are greatly reduced compared to isolated monolayer steps (Akutsu,

2014), the extension of vicinal r-plane edge surfaces could remain rather limited and dolomite might preserve the low energy morphology of the starting rhombohedral crystals. As a result, dissolution rates derived from the kinematic study of smooth cleavage surfaces by AFM might not differ significantly from those obtained from bulk dissolution studies.

5. CONCLUDING REMARKS

The microscopic analysis of dolomite cleavage planes (r-planes) as a function of aqueous solution composition and reaction time showed that surface dissolution fluxes varied by almost one order of magnitude under mildly acidic conditions (e.g., pH ≈ 4.9), reflecting the corresponding heterogeneous distribution of surface energy, whereas the rate variability at basic pH's and high carbonate ion concentrations (pH = 9; $[CO_3^{2-}] \approx 0.3$ mM) was much less pronounced as a consequence of a much lower reactivity of the surface. At these conditions, however, the surface reactivity appeared to be enhanced by the damage induced by surface mechanical treatment, which brought about an increase by a factor of 3 of the mean rate values relative to unpolished cleavage surface. The parallel study of highly kinked c-planes (cut perpendicular to the c-axis) added to the intrinsic variability of dolomite dissolution rates since, at least for short experimental durations, these surfaces were observed to dissolve faster than the r-planes under acidic conditions but slower at basic conditions. The non-quantified implication of steps and kink sites in the edge regions of dolomite crystals complicates the interpretation of dolomite crystal reactivity as a 3D problem, particularly under acidic conditions where the contribution of these sites increased appreciably over the course of the reaction. Moreover, the observed increase of surface roughness did not correspond to an increase of surface reactivity, suggesting that the use of this parameter as a proxy for the density of active sites for dissolution (cf. Schott et al., 2012; Fischer et al., 2014) is not that obvious and should be evaluated case by case.

If on one hand this study provides a detailed characterization of dolomite dissolution behavior as a function of pH and surface orientation and constrains the rate variability under the investigated conditions, on the other hand it also highlights the inherent complexity of the dissolution process and stresses the need for a deeper understanding of the mechanisms that control the dissolution rates of single surfaces and crystals as a whole. The determination of such mechanisms cannot be achieved only by experimental observations but requires the integrated approach of computer modeling to identify processes that current experimental techniques cannot resolve nor quantify alone. Noticeable progress in this respect has been recently achieved by Kinetic Monte Carlo (KMC) simulations (Lüttge and Arvidson, 2010; Lüttge et al., 2013), which promises to be an effective tool to model the evolution of mineral surface topography and the rate distribution resulting from the complex interaction of different elementary mechanisms (cf. Kurganskaya and Lüttge, 2016). However, the advancement of these models and their ability to make

more accurate predictions for systems of increasing complexity rely upon continued experimental work as a means for verification and further development.

ACKNOWLEDGEMENTS

REFERENCES

Akutsu N. (2014) Pinning of steps near equilibrium without impurities, adsorbates or dislocations. *J. Cryst. Growth* **401**, 72–77.

Apps J. A., Zheng L., Zhang Y., Xu T. and Birkholzer J. T. (2010) Evaluation of potential changes in groundwater quality in response to CO_2 leakage from deep geologic storage. *Transport Porous Med.* **82**, 215–246.

Arvidson R. S., Ertan I. E., Amonette J. E. and Lüttge A. (2003) Variation in calcite dissolution rates: a fundamental problem? *Geochim. Cosmochim. Acta* **67**, 1623–1634.

Arvidson R., Beig M. and Luttge A. (2004) Single-crystal plagioclase feldspar dissolution rates measured by vertical scanning interferometry. *Am. Mineral.* **89**, 51–56.

Arvidson R. S. and Lüttge A. (2010) Mineral dissolution kinetics as a function of distance from equilibrium – new experimental results. *Chem. Geol.* **269**, 79–88.

Arvidson R. S., Fischer C. and Lüttge A. (2015) Calcite dissolution kinetics. A comment upon "Evidence and potential implications of exponential tails to concentrations versus time plots for the batch dissolution of calcite by V. M. Truesdale". *Aquat. Geochem.* **21**, 415–422.

Beig M. and Lüttge A. (2006) Albite dissolution kinetics as a function of distance from equilibrium: Implications for natural feldspar weathering. *Geochim. Cosmochim. Acta* **70**, 1402–1420.

Berner R. A., Lasaga A. C. and Garrels R. M. (1983) The carbonate-silicate geochemical cycle and its effect on atmospheric carbon dioxide over the past 100 million years. *Am. J. Sci.* **283**, 641–683.

Bisschop J., Dysthe D. K., Putnis C. V. and Jamtveit B. (2006) In situ AFM study of the dissolution and recrystallization behaviour of polished and stressed calcite surfaces. *Geochim. Cosmochim. Acta* **70**, 1728–1738.

Bonzel H. P. (2003) 3D equilibrium crystal shapes in the new light of STM and AFM. *Phys. Rep.* **385**, 1–67.

Chou L., Garrels R. M. and Wollast R. (1989) Comparative study of the kinetics and mechanisms of dissolution of carbonate minerals. *Chem. Geol.* **78**, 269–282.

Compton R. G., Daly P. J. and Houses W. A. (1986) The dissolution of Iceland spar crystals: the effect of surface morphology. *J. Colloid Interf. Sci.* **113**, 12–20.

Daval D., Hellmann R., Saldi G. D., Wirth R. and Knauss K. G. (2013) Linking nm-scale measurements of the anisotropy of silicate surface reactivity to macroscopic dissolution rate laws: new insights based on diopside. *Geochim. Cosmochim. Acta* **107**, 121–134.

De Giudici G. (2002) Surface control vs. diffusion control during calcite dissolution: dependence of step-edge velocity upon solution pH. *Am. Mineral.* **87**, 1279–1285.

Duckworth O. W. and Martin S. T. (2003) Connections between surface complexation and geometric models of mineral dissolution investigated for rhodochrosite. *Geochim. Cosmochim. Acta* **67**, 1787–1801.

Emmanuel S. (2014) Mechanisms influencing micron and nanometer-scale reaction rate patterns during dolostone dissolution. *Chem. Geol.* **363**, 262–269.

Emmanuel S. and Levenson Y. (2014) Limestone weathering rates accelerated by micron-scale grain detachment. *Geology* **42**(9), 751–754.

Fenter P., Zhang Z., Park C., Sturchio N., Hu X. and Higgins S. R. (2007) Structure and reactivity of the dolomite (104)-water interface: new insights into the dolomite problem. *Geochim. Cosmochim. Acta* **71**, 566–579.

Fischer C., Arvidson R. S. and Lüttge A. (2012) How predictable are dissolution rates of crystalline material? *Geochim. Cosmochim. Acta* **98**, 177–185.

Fischer C., Kurganskaya I., Schäfer T. and Lüttge A. (2014) Variability of crystal surface reactivity: what do we know? *Applied Geochem.* **43**, 132–157.

Fouke B. W. and Reeder R. J. (1992) Surface structural controls on dolomite composition: evidence from sectoral zoning. *Geochim. Cosmochim. Acta* **5656**, 4015–4024.

Gautelier M., Oelkers E. H. and Schott J. (1999) An experimental study of dolomite dissolution rates as a function of pH from-0.5 to 5 and temperature from 25 to 80 °C. *Chem. Geol.* **157**, 13–26.

Godinho J. R. A., Piazolo S. and Evins L. Z. (2012) Effect of surface orientation on dissolution rates and topography of CaF2. *Geochim. Cosmochim. Acta* **86**, 392–403.

Godinho J. R. A., Piazolo S. and Balic-Zunic T. (2014) Importance of surface structure on dissolution of fluorite: implications for surface dynamics and dissolution rates. *Geochim. Cosmochim. Acta* **126**, 398–410.

Hartman P. and Perdok W. G. (1955) On the relations between structure and morphology of crystals. I. *Acta Crystallogr.* **8**, 49–52.

Higgins S. R. and Hu X. (2005) Self-limiting growth on dolomite: experimental observations with in situ atomic force microscopy. *Geochim. Cosmochim. Acta* **69**, 2085–2094.

Higgins S. R., Jordan G. and Eggleston C. (2002) Dissolution kinetics of magnesite in acidic aqueous solution: a hydrothermal atomic force microscopy assessing step kinetics and dissolution flux. *Geochim. Cosmochim. Acta* **66**, 3201–3210.

Hu X., Grossie D. and Higgins S. R. (2005) Growth and dissolution kinetics at the dolomite-water interface: an in-situ scanning probe microscopy study. *Am. Mineral.* **90**, 963–968.

Jordan G. and Rammensee W. (1996) Dissolution rates and activation energy for dissolution of brucite (001): a new method based on the microtopography of crystal surfaces. *Geochim. Cosmochim. Acta* **60**, 5055–5062.

Jordan G. and Rammensee W. (1998) Dissolution rates of calcite (104) obtained by scanning force microscopy: microtopography-based dissolution kinetics on surfaces with anisotropic step velocities. *Geochim. Cosmochim. Acta* **62**, 941–947.

Kaczmarek S. and Sibley D. (2007) A comparison of nanometer-scale growth and dissolution features on natural and synthetic dolomite crystals: implications for the origin of dolomite. *J. Sediment. Res.* **77**, 424–432.

Kaczmarek S. E. and Sibley D. F. (2014) Direct physical evidence of dolomite recrystallization. *Sedimentology* **61**, 1862–1882.

King H. E., Satoh H., Tsukamoto K. and Putnis A. (2014) Surface-specific measurements of olivine dissolution by phase-shift interferometry. *Am. Mineral.* **99**, 377–386.

Klopfstein M. J. and Lucca D. A. (2011) Recent Assessment of surface integrity resulting from fine finishing processes. 1st CIRP Conference on Surface Integrity (CSI). *Procedia Eng.* **19**, 209–221.

Kurganskaya I. and Lüttge A. (2016) Kinetic Monte Carlo approach to study carbonate dissolution. *J. Phys. Chem. C* **120**, 6482–6492.

Lasaga A. and Lüttge A. (2001) Variation of crystal dissolution rate based on a dissolution stepwave model. *Science* **291**, 2400–2404.

Lea A., Amonette J., Baer D., Liang Y. and Colton N. (2001) Microscopic effects of carbonate, manganese, and strontium ions on calcite dissolution. *Geochim. Cosmochim. Acta* **65**, 369–379.

Liang Y. and Baer D. (1997) Anisotropic dissolution at the $CaCO_3$ (1014)-water interface. *Surf. Sci.* **373**, 275–287.

Lucca D. A., Shao L., Wetteland C. J., Misra A., Klopfstein M. J. and Nastasi M. (2006) Subsurface damage in (1 0 0) ZnSe introduced by mechanical polishing. Nucl. Instrum. Methods Phys. Res. *Sect. B* **249**, 907–910.

Lüttge A. (2005) Etch-pit coalescence, surface area, and overall mineral dissolution rates. *Am. Mineral.* **90**, 1776–1783.

Lüttge A., Winkler U. and Lasaga A. (2003) Interferometric study of the dolomite dissolution: a new conceptual model for mineral dissolution. *Geochim. Cosmochim. Acta* **67**, 1099–1116.

Lüttge A., Arvidson R. S. and Fischer C. (2013) A stochastic treatment of crystal dissolution kinetics. *Elements* **9**, 183–188.

Lüttge A. and Arvidson R. S. (2010) Reactions at surfaces: a new approach integrating interferometry and kinetic simulations. *J. Am. Ceram. Soc.* **93**, 3519–3530.

MacInnis I. and Brantley S. (1992) The role of dislocations and surface morphology in calcite dissolution. *Geochim. Cosmochim. Acta* **56**, 1113–1126.

Mackenzie F. T. and Andersson A. J. (2013) The marine carbon system and ocean acidification during Phanerozoic time. *Geochem. Perspect.* **2**, 1–227.

Maher K., Steefel C. I., White A. F. and Stonestrom D. A. (2009) The role of reaction affinity and secondary minerals in regulating chemical weathering rates at the Santa Cruz Soil Chronosequence, California. *Geochim. Cosmochim. Acta* **73**, 2804–2831.

Orton R. and Unwin P. R. (1993) Dolomite dissolution kinetics at low pH: a channel-flow study. *J. Chem. Soc. Faraday Trans.* **89**, 3947–3954.

Paquette J. and Reeder R. J. (1995) Relationship between surface structure, growth mechanism, and trace element incorporation in calcite. *Geochim. Cosmochim. Acta* **59**, 735–749.

Parkhurst D. L. and Appelo C. A. J. (2013). Description of input and examples for PHREEQC version 3—A computer program for speciation, batch-reaction, one-dimensional transport, and inverse geochemical calculations. U.S. Geological Survey Techniques and Methods, book 6, chap. A43, 497 p., available only at <https://pubs.usgs.gov/tm/06/a43/>.

Pokrovsky O., Golubev S. and Jordan G. (2009) Effect of organic and inorganic ligands on calcite and magnesite dissolution rates at 60 °C and 30 atm pCO_2. *Chem. Geol.* **265**, 33–43.

Pokrovsky O. and Schott J. (2001) Kinetics and mechanism of dolomite dissolution in neutral to alkaline solutions revisited. *Am. J. Sci.* **301**, 597–626.

Pollet-Villard M., Daval D., Ackerer P., Saldi G. D., Wild B., Knauss K. G. and Fritz B. (2016) Does crystallographic anisotropy prevent the conventional treatment of aqueous mineral reactivity? A case study based on K-feldspar dissolution kinetics. *Geochim. Cosmochim. Acta* **190**, 294–308.

Putnis C. V., Ruiz-Agudo E. and Hövelmann J. (2014) Coupled fluctuations in element release during dolomite dissolution. *Mineral. Mag.* **78**, 1355–1362.

Ruiz-Agudo E., Urosevic M., Putnis C. V., Rodriguez-Navarro C., Cardell C. and Putnis A. (2011) Ion specific effects on the kinetics of mineral dissolution. *Chem. Geol.* **281**, 364–371.

Schott J., Brantley S., Crerar D., Guy C., Borcsik M. and Willaime C. (1989) Dissolution kinetics of strained calcite. *Geochim. Cosmochim. Acta* **53**, 373–382.

Schott J., Pokrovsky O. S. and Oelkers E. H. (2009) The link between mineral dissolution/precipitation kinetics and solution chemistry. *Rev. Mineral. Geochem.* **70**, 207–258.

Schott J., Oelkers E. H., Bénézeth P., Goddéris Y. and François L. (2012) Can accurate kinetic laws be created to describe chemical weathering? *C. R. Geosci.* **344**, 568–585.

Shiraki R., Rock P. and Casey W. (2000) Dissolution kinetics of calcite in 0.1 M NaCl solution at room temperature: an atomic force microscopic (AFM) study. *Aquat. Geochem.* **66**, 87–108.

Smith M. E., Knauss K. G. and Higgins S. R. (2013) Effects of crystal orientation on the dissolution of calcite by chemical and microscopic analysis. *Chem. Geol.* **360–361**, 10–21.

Teng H. H. (2004) Controls by saturation state on etch pit formation during calcite dissolution. *Geochim. Cosmochim. Acta* **68**, 253–262.

Urosevic M., Rodriguez-Navarro C., Putnis C. V., Cardell C., Putnis A. and Ruiz-Agudo E. (2012) In situ nanoscale observations of the dissolution of dolomite cleavage surfaces. *Geochim. Cosmochim. Acta* **80**, 1–13.

Voltolini M., Artioli G. and Moret M. (2012) The dissolution of laumontite in acidic aqueous solutions: a controlled-temperature in situ atomic force microscopy study. *Am. Mineral.* **97**, 150–158.

White A. and Brantley S. (2003) The effect of time on the weathering of silicate minerals: why do weathering rates differ in the laboratory and field? *Chem. Geol.* **202**, 479–506.

Worthington S. R. H. and Ford D. C. (2009) Self-organized permeability in carbonate aquifers. *Ground Water* **47**, 326–336.

Wunsch A., Navarre-Sitchler A. K., Moore J., Ricko A. and McCray J. E. (2013) Metal release from dolomites at high partial-pressures of CO_2. *Appl. Geochem.* **38**, 33–47.

Xu M., Sullivan K., VanNess G., Knauss K. G. and Higgins S. R. (2013) Dissolution Kinetics and Mechanisms at Dolomite-Water Interfaces: Effects of Electrolyte Specific Ionic Strength. *Environ. Sci. Technol.* **47**, 110–118.

Associate editor: Carl Steefel